A Niccolite Structural Multiferroic Metal–Organic Framework Possessing Four Different Types of Bistability in Response to Dielectric and Magnetic Modulation

Jiong-Peng Zhao, Jian Xu, Song-De Han, Qing-Lun Wang, and Xian-He Bu*

Multiple switchable physical properties have been demonstrated in one single niccolite structural metal–organic framework, [(CH$_3$CH$_2$)$_2$NH$_2$] [Fe^{III}Fe^{II}(HCOO)$_6$] (1), including (i) a reversible ferroelastic phase transition triggered by freezing the disordered (CH$_3$CH$_2$)$_2$NH$_2^+$ cations, (ii) a thermally switchable dielectric constant transition accompanied by phase transition, and (iii) thermal and positive magnetic field driven magnetic poles reversal at low temperatures, attributed to different responses of the magnetization of Fe^{II} and Fe^{III} sublattices to external stimuli. More interestingly, the exchange anisotropy between the two sublattices can also give rise to tunable positive and negative exchange bias fields. Straightforwardly, such diverse demonstrations of bistability in one single material (depending on the specific tuning way) will provide extra freedom and flexibility for the design of switcher devices.

Functional materials featuring sudden change of their physical and/or chemical properties in response to temperature fluctuation, pressure variation, light, electric/magnetic field, and other external stimuli have attracted great attention over the past decade.[1–3] Typically, their responsive dynamics involves two distinct states (i.e., bistability) with regard to color, magnetization, electrical resistance, electrical polarization, or other physical properties, giving rise to potential advantages in the applications of sensors, displays, switches, and especially digital memory devices at a digital age.[4–7] In a sense, developing the materials simultaneously showing multiple types of switchable physical properties, which arise from different physical channels and can be easily tuned in a controlled manner in terms of different trigger mechanisms, could give extra freedom and flexibility for the design of switcher devices. Obviously, this idea is much beneficial to meet the requirement of the rapid development in device technology, but challenging to be implemented.[7]

The spin crossover (SCO) materials that flip between the high spin (HS) and low spin (LS) state when subjected to a physical or chemical stimulus is one of the most known bistable systems.[8,9] Referring to the literature, there also exist two types of bistability in analogy with SCO. One is switchable dielectric constant between the high-dielectric and low-dielectric state, revealed recently in several molecular materials. For example, Jain et al. discovered switchable dielectric constant as a function of temperature in metal formates with perovskite structure.[10,11] Further studies indicate the dipolar reorientation makes a major contribution to the transition between different dielectric states.[12,13] This conclusion then suggests the metal-organic frameworks (MOFs) with mobile guest molecules around the rigid cavities to be a promising candidate for switchable dielectric materials,[14,15] in which the guests can be viewed as electric dipole moments. Importantly, the molecular-based nature of MOF materials not only makes it easy to regulate the structure and dielectric behavior, but also can engraft other physical properties into the systems, which has been rarely reported.
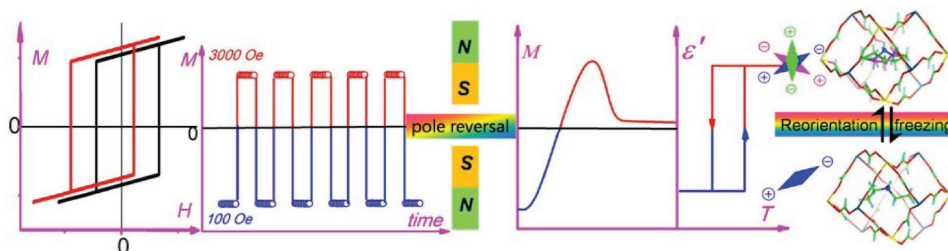
The other bistable system is magnetization reversal, which is defined as a crossover of dc magnetization from a positive value to a negative value as a function of temperature.[16] The magnetization reversal has technological applications in the area of magnetic storage devices, in which two allowed states (positive and negative) of magnetization are needed, but has not yet been paid enough consolidated attention in the literature.[17] More importantly, the negative magnetization under positive applied field provides potential magnetic field to drive the switching of magnetization. To date, most existing switchable materials are thermo switches, wherein the temperature serves as the driving force to flip the two states. In other words, one has to heat or cool the sample across the critical temperature (T_C) to propel the system back toward its original state.[17] In fact, the responsive materials triggered by other stimuli, such

Dr. J.-P. Zhao, Dr. S.-D. Han, Dr. Q.-L. Wang, Prof. X.-H. Bu
State Key Laboratory of Elemento-Organic Chemistry
College of Chemistry
Nankai University
Tianjin 300071, China
E-mail: buxh@nankai.edu.cn
Dr. J.-P. Zhao
School of Chemistry and Chemical Engineering
TKL of Organic Solar Cells and Photochemical Conversion
Tianjin University of Technology
Tianjin 300387, China
Dr. J. Xu, Prof. X.-H. Bu
School of Materials Science and Engineering
TKL of Metal and Molecule-Based Material Chemistry
Collaborative Innovation Center of Chemical Science
and Engineering (Tianjin)
Nankai University
Tianjin 300350, China

**ADVANCED
SCIENCE NEWS**
www.advancedsciencenews.com

**ADVANCED
MATERIALS**
www.advmat.de

Scheme 1. Exchange bias and four different types of bistability in response to magnetic and dielectric modulation coexisting in **1**.

as light, magnetic or electric fields, may be more convenient in use, especially in the application of quickly writing information, but have been less reported by far.[18–21]

Compared with the extensively studied perovskite structural metal formates, some of which exhibit interesting switchable dielectric,[10,11] switchable polarization,[22] and multiferroic properties,[23,24] the most important feature of metal formates with niccolite structure is that it may contain iron in two valence states, which would give rise to more complex and fascinating magnetic properties than those in the perovskites.[25,26] In this regard, a N-type of ferrimagnetism accompanied by order–disorder transitions were revealed in a mixed valence complex $[(CH_3)_2NH_2][Fe^{III}Fe^{II}(HCOO)_6]$.[25–29] Very recently, another interesting example of mixed valence iron formates was reported by Mączka et al.,[30] that is, $[(CH_3CH_2)_2NH_2][Fe^{III}Fe^{II}(HCOO)_6]$ (**1**), which exhibited intriguing crystallographic, magnetic and dielectric behaviors. Going beyond this pioneering work, we herein successfully solved the single crystal structure of **1** at low-temperature phase (LTP) and discovered a ferroelastic phase transition in this complex. More importantly, the positive magnetic field regulated magnetic poles switching and tunable exchange bias were first detected in **1**. Thus, this fascinating compound demonstrates a very rare example of integrating multiple switchable physical properties in one system, including reversible ferroelastic phase transition, switchable dielectric constant transition, thermally and positive magnetic field regulated magnetic poles switching and tunable exchange bias (**Scheme 1**).

The purity of the crystalline sample of **1** was analyzed by infrared radiation (IR) and X-ray powder diffraction (XPRD) (Figures S1 and S2, Supporting Information). Further, a reversible thermal phase transition involving the reorientation of the diethylamine (DEA) cations was confirmed by the differential scanning calorimetry (DSC) (Figure S3, Supporting Information) and variable-temperature single-crystal X-ray diffraction studies. At 293 K, that is, high-temperature phase (HTP), **1** crystallizes in the trigonal space group $P\bar{3}1c$ with the parameter sets of $a^{HTP} = 8.4563(12)$ Å, $c^{HTP} = 13.789(3)$ Å, and $V^{HTP} = 854.0(2)$ Å^3 (Table S1, Supporting Information). A common structural feature of **1** is that its anionic cages formed by $Fe^{II}-HCOO^--Fe^{III}$ units accommodate the DEA cations for charge balance (**Figure 1**a,b), where the valence states of the involved iron ions located at the $(4^{12} \cdot 6^3)$ and $(4^9 \cdot 6^6)$ nodes of the niccolite framework[26] were identified based on the bond lengths: $Fe^{III}-O = 2.0107(15)$ Å and $Fe^{II}-O = 2.1350(16)$ Å (Table S2, Supporting Information). At 113 K (LTP), **1** crystallizes in the triclinic space group $P\bar{1}$, where $a^{LTP} = 8.2974(17)$ Å,

$b^{LTP} = 8.4878(17)$Å, $c^{LTP} = 13.482(3)$ Å, and $V^{LTP} = 835.5(3)$. These lattice parameters are very similar to those reported by Mączka et al., which were solved by using powder diffraction technique and suggested a $P\bar{1}$ or $P1$ symmetry at LTP.[30] Significantly, the present data give a clear evidence for the centrosymmetric $P\bar{1}$ structure at LTP. The reciprocal cells at HTP and LTP follow the relations of $a^{LTP} \approx a^{HTP}$, $b^{LTP} \approx a^{HTP} + b^{HTP}$, $c^{LTP} \approx c^{HTP}$, and $V^{LTP} \approx V^{HTP}$ (Figure 1c). The trivalent Fe^{III} sites at LTP can be classified as two crystallographically independent ions (denoted as Fe2 and Fe3 hereafter), while the coordinated geometry of the divalent Fe^{II} ions, Fe1, exhibits a slight distortion (Table S2, Supporting Information).

Notably, the molecular symmetry of the DEA cation is very different from that of the star molecule, DMA. As known, the DMA cation belongs to C_{2v} point group consisting of four symmetry elements $[E, C_2, \sigma_v(1), \sigma_v(2)]$ (**Figure 2**), while the DEA cation has two conformations: for model I, DEA belongs to C_{2v} point group and thus has the same symmetry elements as those of DMA; for model II, DEA belongs to C_1 point group and thus has only one symmetry element (E). At HTP, the DEA cations have a pseudo D_3 symmetry, sharply differing from the pseudo D_{3h} symmetric of DMA $(NH_2(CH_3)_2)$ cations in isostructural complexes.[25–29] When the dynamic rotations of the guest DEA cations are frozen, the pseudo symmetry is then broken that in turn triggers a phase transition from HTP to LTP. At LTP, the DEA cations adopt the model II conformation, leading to a low symmetry space group $P\bar{1}$, rather than that of DMA in $R\bar{3}c$,[27] since the symmetry of the cation could not be lower than that of the located Wyckoff sites. Thus, besides the impact of metal
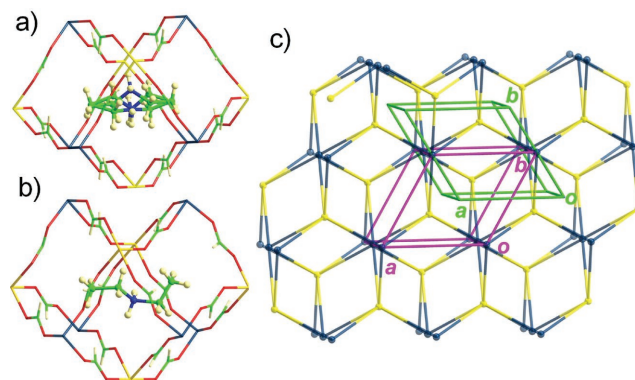

Figure 1. a,b) View of the positions of the disorder and order $[NH_2(CH_2CH_3)_2]$ molecules in the cell of **1** at HTP and LTP; c) Topological views of the framework along the c-axis with the unit cells in HTP (pink box) and LTP (green box).
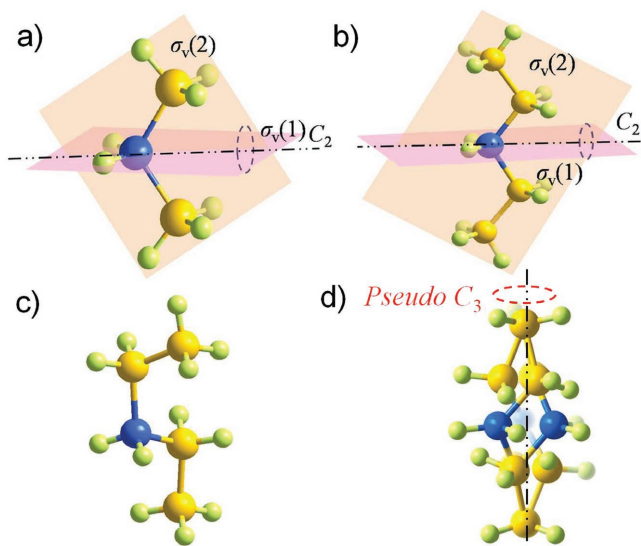
Figure 2. a) Conformation and symmetry elements of the DMA cation; b,c) Conformation and symmetry elements of the DEA cation for model I and for model II; d) Proposed rotation models for the DEA at HTP.

ions in niccolite structural metal formates,[27,31,32] the symmetry of the cation itself should also be taken into account in the total decrease of the symmetry elements during the phase transition. In **1**, along with the phase transition from $P\bar{3}1c$ to $P\bar{1}$, the total number of the symmetry elements of the crystallographic point group decreases from 12 (E, $2C_3$, $3C_2$, i, $2S_6$, $3\sigma_v$) to 2 (E, i) (Figure S4, Supporting Information), suggesting a ferroelastic phase transition with an *Aizu* notation of $3mF\bar{1}$.[33] And the maximal non-isomorphic subgroups of paraelastic phase of **1** at HTP are 3m, 32, $\bar{3}$, 2/m, respectively, while the groups $\bar{3}$ and 2/m comprise the one in ferroelastic phase at LTP ($\bar{1}$).

Variable-temperature (VT) dielectric spectra were measured on the single crystal of **1** in the temperature range of 175–270 K (**Figure 3**), in which the electric field was perpendicular to the *c*-direction. The results clearly reveal that the high-dielectric state exists in paraelastic phase, while the low-dielectric state in ferroelastic phase, which should be attributed to the static-motional transitions of the polar DEA cations in the crystal,
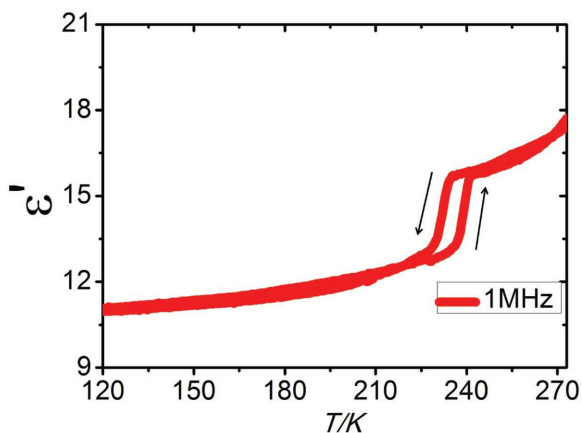

Figure 3. Temperature dependence of the real part of dielectric constant of single crystal of **1** at 1 MHz.

suggesting the occurrence of an order–disorder phase transition between LTP and HTP.[12] The plots of ε' versus T reveal an obvious hysteresis between the cooling and heating processes at about 227–240 K. The peak range of ε' agrees with that of the DSC measurement. The DSC peak temperatures in cooling and heating processes are about 234 and 240 K, respectively, being slightly smaller than that of 237 and 242 K reported by Maczka et al.,[30] which is due to the discrepancy in the heating/cooling rates. Also, all these plots show little frequency dependence in the measured frequency range of 5K–1M Hz, indicating that the polar motions are much faster than 1 MHz (Figure S5, Supporting Information). Evidently, the dielectric data measured from the single crystal sample of **1** are steeper than that from the powder samples (Figure S5b, Supporting Information) as well as that reported by Maczka et al.[30] This phenomenon should be ascribed to the freezing of the DEA cations around the *c*-direction at HTP, which could give rise to an anisotropic dielectric behavior.[12–15]

Variable-temperature magnetic susceptibility, zero field cooling magnetization, and field cooling magnetization (**Figure 4** and Figures S6–S8, Supporting Information) reveal the N-type ferrimagnet nature of **1** with T_N and T_{comp} (compensation temperature) being about 38 and 20 K. To be noted, the T_N and T_{comp} values are very similar to those reported by Maczka et al.[30] The compensation effect should be due to the fact that the sublattice with smaller saturation magnetization initially orders more rapidly than that with larger saturation magnetization. Meanwhile, a very large negative magnetization was also found below 20 K under a low applied field, which is very rare for molecular-based magnets.[34–36] In **1**, the magnetization of the Fe^{II} sublattices under the applied field orders faster than that of the Fe^{III} ion and the single-ion anisotropy arising from the spin–orbit coupling makes the orientation of the Fe^{II} moments exert on the larger molecular field when the temperature lowers below T_C. Thus, under a small applied field, the barrier due to the anisotropy effect is sufficient to hinder the occurrence of magnetization reversal, which consequently leads to a negative magnetization below T_{comp}. So, whenever the applied field is strong enough to compensate this anisotropy effect, the magnetization will then decrease from the maximum upon cooling, along with a reorientation of the magnetizations of the two sublattices, but without magnetic pole reversal. It is worth noting that negative magnetization was also found in a mixed valence formate with $CH_3CH_2NH_3^+$ cations, which, however, exhibited no obvious structure transition.[30]

More importantly, a manifestation of the bipolar switching of the magnetization of **1** at 16 K when varying the magnitude of the positive applied field was given in **Figure 5**a. In this experiment, the samples were initially cooled across T_N to 16 K upon an external magnetic field of 100 Oe with $M = -130$ emu mol^{-1}. An initial positive magnetization of 100 emu mol^{-1} can be gained by increasing H to 3000 Oe at a fixed temperature, and the bipolar switching can be realized by subsequently alternating H between 100 and 3000 Oe. This then suggests that after a field cooling with a negative magnetization below T_{comp}, the moment of the Fe^{II} sublattice is frozen, while the orientation of the Fe^{III} moments depends closely on the antiferromagnetic (AF) interactions between the two sublattices and the strength of the applied field (Figure 5b). So, if
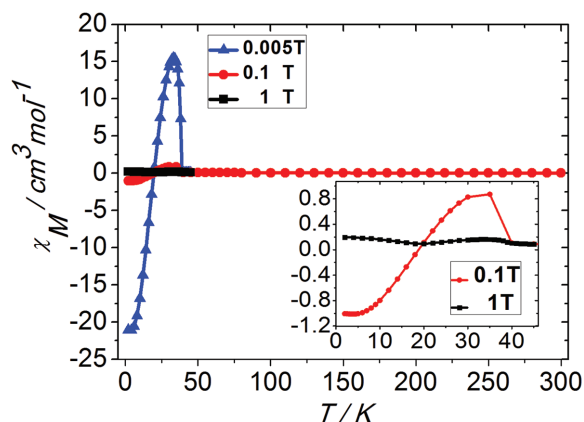
**ADVANCED
SCIENCE NEWS**
www.advancedsciencenews.com

**ADVANCED
MATERIALS**
www.advmat.de

Figure 4. Field-cooled (FC) magnetization for **1** at different applied fields. Inset: The FC magnetization with applied fields of 0.1 and 1 T at 2–45 K.

the strength of the applied field was sufficiently large compared to the AF interactions, the reorientation of the Fe^{III} moments could take place, which would cause the whole magnetization to flip from negative to positive. And when the applied field decreases to a small value, the AF interactions and the anisotropy of the Fe^{II} sublattice would then cause the magnetization to revert back to the initial negative value. Evidently, the bipolar switching of magnetization can be achieved in such a way by just varying the magnitude of the positive applied field. Importantly, such a field magnitude variation induces the magnetization cycles between negative and positive values, that is, a reversible bipolar switching, without any observable decay in magnitude. The magnetic bistability, which refers to the sudden reorientations of the spin following the change of the applied field, has been extensively studied in spin-frustration systems.[37,38] However, a reversible bipolar switching realized by simply regulating the strength of positive field is very rare in the literature[18,39] despite several materials show the similar temperature-dependent magnetization reversal.[17,34–36] Significantly, the observed magnetic pole reversal behavior of this complex demonstrates its feasibility in the applications of magnetic data storage and switches, that is, the thermo-magnetic switch and volatile magnetic memories. Further, the field-driven magnetic polar reversal is obviously more convenient than the thermo-magnetic switches, because the latter has to heat or cool the sample across T_C to propel the system back to its original state to accomplish the reversal between two magnetic states.

The freezing of the Fe^{II} spins is also confirmed by the magnetization hysteresis behavior between −4000 and 5500 Oe at 16 K (Figure 5c). The magnetic loop is asymmetric and shifts toward positive field axis, indicative of the presence of another magnetic field (H_i) in addition to the applied one (H_a). This is a

typical exchange bias phenomenon and occurred under a bias field of $H_{EB} = 1828$ Oe ($H_{EB} = (H_+ + H_-)/2$), in which H_+ and H_- are the field values corresponding to $M = 0$ at the ascending and descending branches of the hysteresis loop, respectively. Moreover, the magnetic moment (μ_i) of the Fe^{II} spins responsible for the internal magnetic field (H_i) and reversal of μ_i does not occur for $H_a \leq 5500$ Oe at $T = 16$ K, while the reversal of μ_i at 16 K can take place only under large H_a (e.g., $H_a = 5$ T). The hysteresis loops were also recorded under the FC condition (with 0.01 and 1 T) between −5 and 5 T at 16 K. It is clear to see that these loops are symmetric, which indicates the reversal of the Fe^{II} spins under large fields (Figure 5d and Figure S9a, Supporting Information).

Further, from Figure S9b (Supporting Information), we find that the Fe^{II} spins refreeze gradually under the increasing demagnetization fields, where the magnetizations of the demagnetization process increase in the case of large starting demagnetization fields. Evidently, the field for the reversal of the magnetic pole is temperature dependent: after a 1000 Oe field cooling (at 5 K), the switching of the negative magnetization to positive one requires a positive field value of 6000 Oe. With the field as such strength, the Fe^{II} spins could also flip, however, the magnetization would not change to be negative again when the field decreased to the initial value (Figure S10, Supporting Information). It is worth noticing that another magnetic moment (μ_i) containing high anisotropy was generated at 2 K during a field cooling process under a larger applied filed. At 2 K, the hysteresis loops were recorded under FC condition with the external fields of 0.01, 0.1, 1, and −1 T. It was observed that with the small cooling fields, that is, 0.01 and 0.1 T, the loop is symmetric (Figure S11, Supporting Information) and
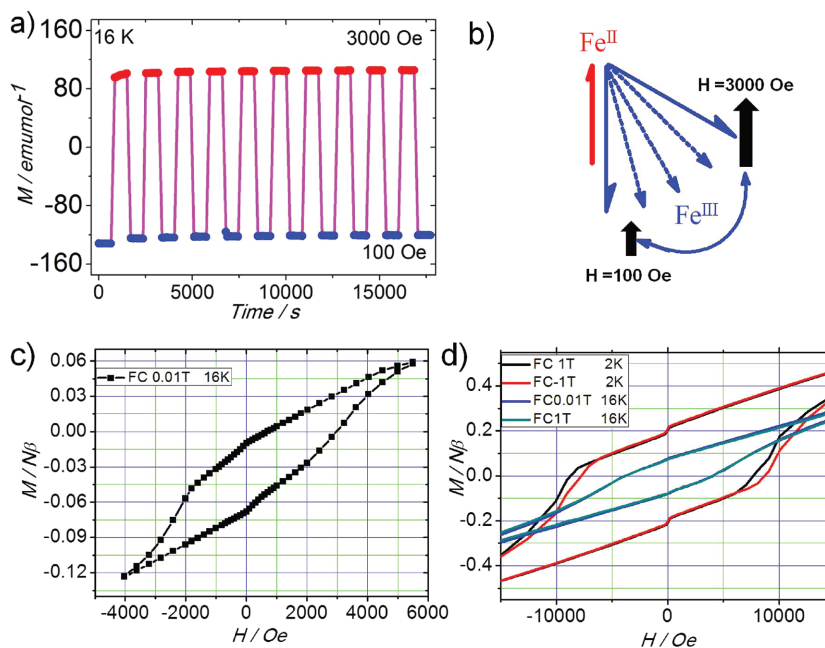

Figure 5. a) Bipolar switching of magnetization for **1** at 16 K under 100 and 3000 Oe flipped magnetic field; b) Schematic representation of the response of the Fe^{II} and Fe^{III} moments under applied varying field at 16 K; c) M–H loops recorded at 16 K for **1** after a 100 Oe field cooling with a field variation between −4000 and 5500 Oe; d) Enlarged part of M–H loops recorded at 2 and 16 K for **1** after different cooling fields with a field variation between −5 and 5 T.

**ADVANCED
SCIENCE NEWS**

www.advancedsciencenews.com

**ADVANCED
MATERIALS**

www.advmat.de

with larger cooling field of 1 T, the coercivity of the ascending branches decreases (Figure 5d and Figure S11, Supporting Information), while that of the descending branches is almost coincident with the one cooled under the field of 0.01 or 0.1 T. Under the cooling condition of −1 T, the coercivity of the descending branches decreases, implying the loop shifts opposed to the applied field upon cooling. Since the bias field in **1** is negative, which is different from the DMA-templated complex,[26] the origin of μ_i generated upon high cooling field at 2 K need to be further explored.

In summary, we have demonstrated the reversible disorder–order ferroelastic phase transition in a niccolite structural MOF, $[(CH_3CH_2)_2NH_2][Fe^{III}Fe^{II}(HCOO)_6]$ (**1**). The impact of the symmetry of guests on the phase transition was discussed. The switchable dielectric constant due to the drastic changes of the motion of DEA cations was revealed in **1**. Magnetic studies indicated a thermal and positive magnetic field driven magnetic poles reversal and the tunable exchange bias in **1**. The highly reversible bipolar switching of magnetization is distinct from the nonreversible rotation of ferro/ferrimagnetic domains by applying external magnetic fields. The presence of two or more distinct switchable physical natures, for example, dielectric constant and magnetization polarization, in one crystalline complex is of peculiar significance for the applications of high density information storage and multiple logic gates. In addition, the potential couplings between structures, mechanics, exchange bias, magnetic and dielectric properties in the new phase transition material in quest for multiferroics are worth further investigation.

Experimental Section

Materials and Methods: All chemicals were reagent grade and used as purchased without further purification. The XRPD spectra were recorded on a Rigaku D/Max-2500 diffractometer at 40 kV, 100 mA for a Cu-target tube and a graphite monochromator. IR spectra were measured in the range of 400–4000 cm^{-1} on a Tensor 27 OPUS FT-IR spectrometer using KBr pellets (Bruker, German). Elemental analyses (C, H, N) were performed on a Perkin-Elmer 240C analyzer. Simulation of the XRPD spectrum was carried out by the single-crystal data and diffraction-crystal module of the Mercury (Hg) program (available free of charge at http://www.iucr.org). DSC measurements were performed on a NETZSCH Analyzing under nitrogen at atmospheric pressure with a heating/cooling rate of 10 K min^{-1}. Dielectric constant was measured with a Tonghui TH2828A impedance analyzer over the frequency range of 500 Hz to 1 MHz at a heating/cooling rate of ≈5 K min^{-1} from 120 to 270 K. Magnetic susceptibility was measured by a Quantum Design MPMS superconducting quantum interference device (SQUID). Diamagnetic corrections were estimated by using Pascal constants and background corrections by experimental measurement on sample holders.

X-Ray Crystallography: The crystal structure data in the high-temperature phase were first collected using the Rigaku SCX-mini diffractometer at 293 (2) K with MoKα radiation (λ = 0.71073 Å) by ω scan mode. And later in low-temperature phase at 113(2) K the Rigaku MSC was used. The program CrystalClear[40] was used for the integration of the diffraction profiles. The structure was solved by direct method using the SHELXS program of the SHELXTL package and refined by full-matrix least-squares methods with SHELXL (semiempirical absorption corrections were applied by using the SADABS program).[41] The nonhydrogen atoms were located in successive difference Fourier syntheses and refined with anisotropic thermal parameters on F^2. All hydrogen atoms were generated theoretically at the specific atoms and refined isotropically with fixed thermal factors. The corresponding structural data are summarized in Table S1 (Supporting Information), with selected bond lengths and angles given in Table S2 (Supporting Information). CCDC numbers are 1475874–1475875 for **1** at high and low temperature.

Synthesis of **1**: The block crystals of compound **1** were synthesized by solvothermal reaction of $FeCl_3 \cdot 6H_2O$ (2.5 mmol) in mixed solution containing water, formate acid, and *N,N*-diethylformamide 10 mL with a volume ratio of about 0.5:1:1. The mixture was sealed in a Teflon-lined stainless steel vessel, heated at 140 °C for 2 d under autogenous pressure, and then cooled to room temperature in 36 h. Black hexagonal prism like crystals of **1** with size of about $0.5 \times 0.5 \times 1$ to $2 \times 2 \times 4$ mm^3 were harvested in about ≈40% yield based on $FeCl_3 \cdot 6H_2O$. Elemental analysis (%) calcd for **1**, $C_{10}H_{18}NFe_2O_{12}$ (455.94): C 26.34, H 3.98, N 3.07%; found for **1**: C 26.46, H 3.72, N 3.21%.

Supporting Information

Supporting Information is available from the Wiley Online Library or from the author.

Conflict of Interest

The authors declare no conflict of interest.

[1] E. Coronado, G. M. Espallargas, *Chem. Soc. Rev.* **2013**, *42*, 1525.

[2] S. Matsumoto, T. Higashiyama, H. Akutsu, S. Nakatsuji, *Angew. Chem., Int. Ed.* **2011**, *50*, 10879.

[3] M. Herder, B. M. Schmidt, L. Grubert, M. Pätzel, J. Schwarz, S. Hecht, *J. Am. Chem. Soc.* **2015**, *137*, 2738.

[4] G. Szalóki, G. Sevez, J. Berthet, J. L. Pozzo, S. Delbaere, *J. Am. Chem. Soc.* **2014**, *136*, 13510.

[5] O. Sato, J. Tao, Y. Z. Zhang, *Angew. Chem., Int. Ed.* **2007**, *46*, 2152.

[6] T. T. T. Nguyen, D. Trp, M. Wagner, K. Müllen, *Angew. Chem., Int. Ed.* **2013**, *52*, 669.

[7] Y. Zhang, H. Y. Ye, H. L. Cai, D. W. Fu, Q. Ye, W. Zhang, Q. H. Zou, J. L. Wang, G. L. Yuan, R. G. Xiong, *Adv. Mater.* **2014**, *26*, 4515.

[8] G. J. Halder, C. J. Kepert, B. Moubaraki, K. S. Murray, J. D. Cashion, *Science* **2002**, *298*, 1762.

[9] M. C. Mñnoz, J. A. Real, *Coord. Chem. Rev.* **2011**, *255*, 2068 and references cited therein.

[10] P. Jain, N. S. Dalal, B. H. Toby, H. W. Kroto, A. K. Cheetham, *J. Am. Chem. Soc.* **2008**, *130*, 10450.

[11] P. Jain, V. Ramachandran, R. J. Clark, H. Zhou, B. H. Toby, N. S. Dalal, H. W. Kroto, A. K. Cheetham, *J. Am. Chem. Soc.* **2009**, *131*, 13625.

[12] W. Zhang, H. Y. Ye, R. Graf, H. W. Spiess, Y. F. Yao, R. Q. Zhu, R. G. Xiong, *J. Am. Chem. Soc.* **2013**, *135*, 5230.

[13] C. Shi, X. Zhang, Y. Cai, Y. F. Yao, W. Zhang, *Angew. Chem., Int. Ed.* **2015**, *54*, 6206.

[14] Z. Y. Du, T. T. Xu, B. Huang, Y. J. Su, W. Xue, C. T. He, W. X. Zhang, X. M. Chen, *Angew. Chem., Int. Ed.* **2014**, *53*, 914.

[15] R. Shang, Z. M. Wang, S. Gao, *Angew. Chem., Int. Ed.* **2015**, *54*, 2534.

[16] O. Kahn, *Nature* **1999**, *399*, 21.

[17] A. Kumar, M. S. Yusuf, *Phys. Rep.* **2015**, *556*, 1.

[18] S. M. Yusuf, A. Kumar, J. V. Yakhmi, *Appl. Phys. Lett.* **2009**, *95*, 182506.

[19] S. M. Yoon, S. C. Warren, B. A. Grzybowski, *Angew. Chem., Int. Ed.* **2014**, *534437*.

[20] L. Pan, G. Liu, H. Li, S. Meng, L. Han, J. Shang, B. Chen, A. E. Platero-Prats, W. Lu, X. D. Zou, R. W. Li, *J. Am. Chem. Soc.* **2014**, *136*, 17477.

[21] S. B. Han, S. C. Warren, S. M. Yoon, C. D. Malliakas, X. L. Hou, Y. H. Wei, M. G. Kanatzidis, B. A. Grzybowski, *J. Am. Chem. Soc.* **2015**, *137*, 8169.

[22] P. Jain, A. Stroppa, D. Nabok, A. Marino, A. Rubano, D. Paparo, M. Matsubara, H. Nakotte, M. Fiebig, S. Picozzi, E. S. Choi, A. K. Cheetham, C. Drax, N. S. Dalal, V. S. Zapf, *NPJ Quantum Mater.* **2016**, *1*, 16012.

[23] W. Li, Z. Zhang, E. G. Bithell, A. S. Batsanov, P. T. Barton, P. J. Saines, P. Jain, C. J. Howard, M. A. Carpenter, A. K. Cheetham, *Acta Mater.* **2013**, *61*, 4928.

[24] W. Li, Z. Wang, F. Deschler, S. Gao, R. H. Friend, A. K. Cheetham, *Nat. Rev. Mater.* **2017**, *2*, 16099.

[25] K. S. Hagen, S. G. Naik, B. H. Huynh, A. Masello, G. Christou, *J. Am. Chem. Soc.* **2009**, *113*, 7516.

[26] J. P. Zhao, B. W. Hu, F. Lloret, J. Tao, Q. Yang, X. F. Zhang, X. H. Bu, *Inorg. Chem.* **2010**, *49*, 10390.

[27] L. C. Delgado, O. Fabelo, J. A. R. Velamazán, M. H. L. Cailleau, S. A. Mason, E. Pardo, F. Lloret, J. P. Zhao, X. H. Bu, V. Simonet, C. V. Colin, J. R. Carvajal, *J. Am. Chem. Soc.* **2012**, *134*, 19772.

[28] A. Sieradzki, S. Pawlus, S. N. Tripathy, A. Gągor, A. Ciupa, M. Mączka, M. Paluch, *Phys. Chem. Chem. Phys.* **2016**, *18*, 8462.

[29] A. Ciupa, M. Maczka, A. Gagor, A. Sieradzki, J. Trzmiel, A. Pikula, M. Ptaka, *Dalton Trans.* **2015**, *44*, 8846.

[30] M. Mączka, A. Ciupa, A. Gągor, A. Sieradzki, A. Pikul, M. Ptaka, *J. Mater. Chem. C.* **2016**, *4*, 1186.

[31] L. Mazzuca, L. Cañadillas-Delgado, J. A. Rodríguez-Velamazán, O. Fabelo, M. Scarrozza, A. Stroppa, S. Picozzi, J.-P. Zhao, X.-H. Bu, J. Rodríguez-Carvajal, *Inorg. Chem.* **2017**, *56*, 197.

[32] R. Shang, S. Chen, K.-L. Hu, B.-W. Wang, Z.-M. Wang, S. Gao, *Chem. Eur. J.* **2016**, *22*, 6199.

[33] K. Aizu, *J. Phys. Soc.* **1969**, *27*, 387.

[34] C. J. Nuttall, P. Day, *Chem. Mater.* **1998**, *10*, 3050.

[35] S. Ohkoshi, K. Hashimoto, *J. Am. Chem. Soc.* **1999**, *121*, 10591.

[36] H. Ōkawa, M. Sadakiyo, T. Yamada, M. Maesato, M. Ohba, H. Kitagawa, *J. Am. Chem. Soc.* **2013**, *135*, 2256.

[37] S. M. Humphrey, P. T. Wood, *J. Am. Chem. Soc.* **2004**, *126*, 13236.

[38] W. L. Queen, S.-J. Hwu, L. Wang, *Angew. Chem., Int. Ed.* **2007**, *46*, 5344.

[39] T. Bora, S. Ravi, *J. Magn. Magn. Mater.* **2015**, *386*, 85.

[40] CrystalClear and CrystalStructure, Rigaku/MSC, The Woodlands, TX, USA **2005**.

[41] G. M. Sheldrick, *SHELXL97, Program for Structure Refinement*, University of Göttingen, Göttingen, Germany **1997**.